

A new method for cross-calibration of two satellite sensors

J.-J. LIU*, Z. LI†

Department of Meteorology and ESSIC, University of Maryland, 2207 CSS Building, College Park, MD 20742, USA

Y.-L. QIAO

Anhui Institute of Optical and Fine Mechanics, Chinese Academy of Sciences, Hefei, Anhui, China

Y.-J. LIU and Y.-X. ZHANG

National Satellite Meteorology Center, China Meteorological Administration, Beijing, China

(Received 9 August 2003; in final form 5 May 2004)

Abstract. Given that many operational satellite sensors are not calibrated, while a handful of research sensors are, cross-calibration between the two types of sensor is a cost-effective means of calibration. A new method of sensor cross-calibration is demonstrated here using the Chinese Multi-channel Visible Infrared Scanning radiometer (MVIRS) and the US Moderate Resolution Imaging Spectrometer (MODIS). MVIRS has six channels, equivalent to the current National Oceanic and Atmospheric Administration's (NOAA) Advanced Very High Resolution Radiometer (AVHRR) and four additional ones for remote sensing of ocean colour and moisture. The MVIRS on-board China's polar-orbiting meteorological satellite (FY-1D) was launched on 15 May 2002 with an earlier overpass time than Terra. The sensor has no on-board calibration assembly. This study attempts to calibrate MVIRS against the well-calibrated MODIS, by taking a series of measures to account for their differences. Clear-sky measurements made from the two sensors in July–October 2002 were first collocated. Using the 6S radiative transfer model, MODIS reflectances measured at the top-of-the atmosphere were converted into surface reflectances. They were corrected to the viewing geometry of the MVIRS using the bidirectional reflectance distribution function (BRDF) measured on the ground. The spectral response functions of the two sensors were employed to account for spectral discrepancies. After these corrections, very close linear correlations were found between radiances estimated from the MODIS and the digital readings from the MVIRS, from which the calibration gains were derived. The gains differ considerably from the pre-launch values and are subject to degradation over time. The calibration accuracy is estimated to be less than 5%, which is compatible to that obtained by the more expensive vicarious calibration approach.

*Currently at the National Satellite Meteorology Center, China Meteorological Administration, Beijing, China.

†Corresponding author; e-mail: zli@atmos.umd.edu

1. Introduction

China is one of the few countries in the world that has launched and operated meteorological satellites. China has both sun-synchronous and geostationary satellites denoted as the FY-1 and FY-2 series, respectively. In the FY-1 series, the Multi-channel Visible Infrared Scanning radiometers (MVIRS) on-board the FY-1C and the FY-1D are currently in operation as the primary sensor. They were launched on 10 May 1999 and 15 May 2002, and are in good working condition. The MVIRS has similar channels to the National Oceanic and Atmospheric Administration's (NOAA) Advanced Very High Resolution Radiometer (AVHRR) and includes four extra channels. Table 1 lists all the channels and their primary utility. The first six channels are essentially identical to the current generation of AVHRR radiometers (e.g. NOAA-16). The four additional channels are used to measure ocean colour and water vapour. The instantaneous field-of-view (IFOV) of the MVIRS is 1.2 mrad corresponding to a ground resolution of 1.1 km at nadir. The scan rate is six lines per second and the total number of pixels in each scan line is 2048. Data transmission is so similar to NOAA's High Resolution Picture Transmission (HRPT) that any AVHRR station may acquire and process MVIRS data with minor modifications.

Like AVHRR, MVIRS has no on-board calibration system for the reflectance solar channels. But unlike AVHRR for which extensive post-launch vicarious calibration attempts were made (e.g. Teillet *et al.* 1990, Kaufman and Holben 1993, Rao and Chen 1995, Vermote and Kaufman 1995, Gutman 1999), no post-launch calibration results for the MVIRS on-board FY-1D have been published. There are many approaches for vicarious calibration and state-of-the-art of the methods and procedures are summarized in Slater *et al.* (1996). Radiometric calibration is essential to make quantitative use of the data that can be received at any AVHRR receiving station. Differences in the overpass time make it complementary to other similar imaging sensors.

China conducted a few vicarious calibration campaigns at two primary calibration sites, namely the Qinghai Lake Site and the Dunhuang Site in the Gobi desert from the mid to late 1990s (before FY-1D was launched). These calibration sites were selected following an extensive survey of many potential sites carried out during 1994–1996. A small region in the Gobi desert was selected for calibrating the solar reflectance channels. The site is about 30 km west of Dunhuang City in Gansu Province, a small but famous historical city in western China. The selection stems

Table 1. The characteristics of MVIRS channels on-board FY-1C and FY-1D.

| Channel | Wavelength (μm) | Primary use |
|---------|------------------------------|---|
| 1 | 0.58–0.68 | Daytime cloud, ice and snow, vegetation |
| 2 | 0.84–0.89 | Daytime cloud, vegetation |
| 3 | 3.55–3.95 | Heat source, night cloud |
| 4 | 10.3–11.3 | SST, day/night cloud |
| 5 | 11.5–12.5 | SST, day/night cloud |
| 6 | 1.58–1.64 | Soil moisture, ice/snow distinguishing |
| 7 | 0.43–0.48 | Ocean colour |
| 8 | 0.48–0.53 | Ocean colour |
| 9 | 0.53–0.58 | Ocean colour |
| 10 | 0.90–0.985 | Water vapour |

SST, sea surface temperature.

from the following considerations. First, the area of about 30 km by 50 km is very uniform and flat. The standard deviation of surface reflectance across the central portion of this area is less than 2%. Second, the Gobi desert has no vegetation and thus the surface remains invariant throughout the year, except for rare events of rainfall and snowfall (the mean annual precipitation is 34 mm). Third, it is far from any major sources of air pollution, but reasonably close to Dunhuang city for logistic reasons (Xiao *et al.* 2001, Yi *et al.* 2001, Hu *et al.* 2001a)

Led by the China Meteorological Administration with participants from seven Chinese ministries, a major calibration undertaking was carried out by a team of Chinese scientists from 1997–2001. Two intensive observation campaigns (IOCs) were conducted (June–August 1999 and August–September 2000) in order to calibrate three Chinese satellites: the FY-1C, the FY-2B and the China Brazil Earth Resource Satellite (CBERS-1). During the IOCs, extensive meteorological and radiometric measurements were acquired from the surface and from aircraft. Many high-resolution samples (400 nm–2500 nm) were acquired of surface spectral reflectance and bidirectional reflectance distribution function (BRDF) by ground-based and air-borne spectrometers.

Figure 1 is an example of the surface reflectance spectrum that varies smoothly with wavelengths from less than 15% to above 30%. The large fluctuations at about 1400 nm, 1850 nm and 2450 nm are due to H₂O absorption. Radiances or apparent reflectances of the MVIRS channels at the top-of-the-atmosphere (TOA) were computed by substituting surface and atmospheric variables (reflectance or radiance, aerosol, temperature, humidity, etc.) as measured on the ground and/or from aircraft into the 6S radiative transfer model (Vermote *et al.* 1997). Satellite calibration coefficients were obtained by combining the predicted radiances and the satellite digital readings (Liu *et al.* 2001, Hu *et al.* 2001). It was found that the gain for the FY-1C had degraded significantly from its pre-launch value (table 2). The uncertainty of the calibration results is about 4% to 6% for the visible/near-infrared and short wavelength infrared bands and varies with the methods used (Liu *et al.* 2001, Hu *et al.* 2001b, Zhang *et al.* 2001).

Note that such a vicarious calibration approach is sound but is costly and time

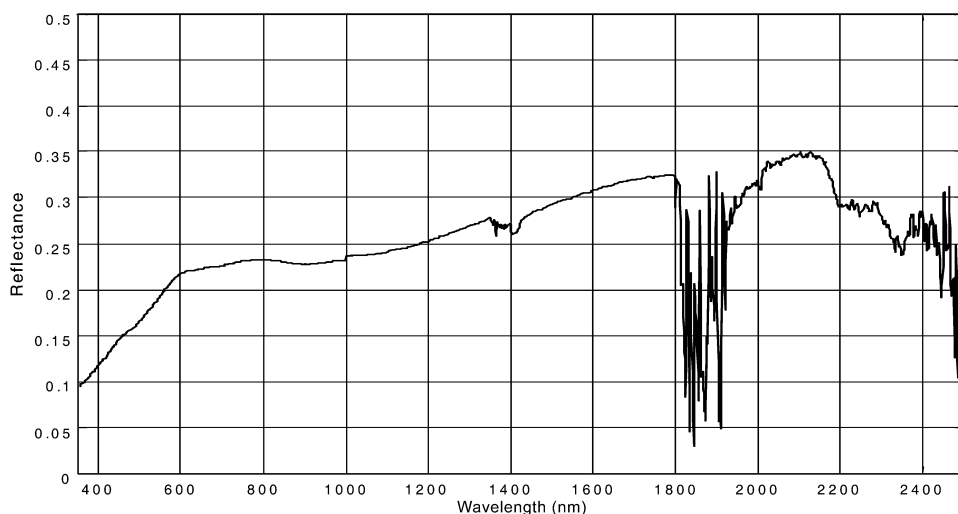


Figure 1. Spectral albedo of Dunhuang site measured at 13:09, 2 July 1999.

Table 2. The calibration gain for determining the apparent reflectance of FY-1C (Hu *et al.* 2001).

| Date | Band 1 | Band 2 | Band 6 | Band 7 | Band 8 | Band 9 | Band 10 |
|------------|--------|--------|--------|--------|--------|--------|---------|
| Pre-launch | 0.0918 | 0.0923 | 0.0840 | 0.0526 | 0.0536 | 0.0537 | 0.0952 |
| 99.7.7 | 0.0829 | 0.0892 | 0.0598 | 0.0483 | 0.0479 | 0.0777 | 0.0902 |
| 99.7.17 | 0.0812 | 0.0912 | 0.0618 | 0.0475 | 0.0470 | 0.0760 | 0.0939 |
| 00.9.14 | 0.1154 | 0.0806 | 0.0665 | 0.0658 | 0.0608 | 0.0815 | 0.0822 |
| Degrade | -20.5% | 14.5% | 26.3% | -20.1% | -11.8% | -34.1% | 15.8% |

consuming. As a result, a cross-calibration method is attempted here to calibrate the FY-1D solar reflectance channels against a well-calibrated satellite sensor, NASA's Moderate Resolution Imaging Spectroradiometer (MODIS) (Barbieri 1997). The method can circumvent the rigid requirement of acquiring simultaneous observations of many atmospheric and surface variables. It is thus more feasible to regularly update the calibration coefficients, as long as a high calibration standard of the reference sensor is maintained. The quality of MODIS calibration is assured by both on-board calibration and ensuing vicarious calibration that may be delayed by three months (Slater and Biggar 1996). Use of field data is necessary to reduce calibration uncertainties. It is worth noting that the paper is focused more on demonstration of the method than an attempt at routine calibration.

2. Datasets

Collocated data from the Terra MODIS and the FY-1D MVIRS sensors acquired over the Dunhuang calibration site are employed in this study. Unlike many other satellite sensors, MODIS is calibrated on-board with a very high signal-to-noise ratio (1000:1 for many solar bands) (Barnes *et al.* 1998). The MODIS solar bands (bands 1–19, and 26 with wavelengths ranging from 0.412 μm to 2.1 μm) were calibrated onboard by a solar diffuser (SD). The degradation of the SD is tracked using a solar diffuser stability monitor. Bands 20–25 and 27–36 (with wavelengths ranging from 3.75 μm to 14.5 μm) are the thermal emissive bands and are calibrated on-orbit by a blackbody (Xiong *et al.* 2003). In addition to the onboard calibrators, observations of the Moon were carefully made under selected viewing conditions (Lyu and Barnes 2003). These observations were used to anchor the on-orbit calibration and characterization (Xiong *et al.* 2003, Barnes *et al.* 2003).

Table 3. The specifications of MODIS bands used in cross calibration.

| Band | λ | IFOV | Bandwidth | Calibration uncertainty |
|------|-----------|--------|-----------|-------------------------|
| 1 | 645 nm | 250 m | 50 nm | |
| 2 | 858 nm | 250 m | 35 nm | |
| 3 | 469 nm | 500 m | 20 nm | |
| 4 | 555 nm | 500 m | 20 nm | |
| 5 | 1240 nm | 500 m | 20 nm | 2.9% |
| 6 | 1640 nm | 500 m | 24.6 nm | |
| 7 | 2130 nm | 500 m | 50 nm | 2.8% |
| 8 | 412 nm | 1000 m | 15 nm | 2.2% |
| 9 | 443 nm | 1000 m | 10 nm | |
| 10 | 488 nm | 1000 m | 10 nm | |

The current estimates of calibration uncertainty for three MODIS solar bands are shown in table 3.

The Terra overpass time (about 4:00–5:00 UTC) and IFOV are close to those of the FY-1Ds (about 3:00 UTC). The numerous MODIS channels of narrow bandwidth allow the interpolation of the spectral reflectance to be more compatible with the MVIRS channels.

Although we do not rely on *in situ* observations for our calibration, pixels over the Dunhuang site were selected for two reasons. First, the surface uniformity lessens the impact of any misregistration between the two datasets. Second, the Gobi desert has a weak BRDF effect. The BRDF was measured during a calibration campaign and used here for correcting reflectance measurements made from one direction to another. Though the effect is weak relative to many other terrestrial targets, it is significant enough that it must be taken into account to achieve an acceptable accuracy for the calibration, as demonstrated below. Third, the region has unique characteristics in favour of calibration, such as low aerosol loading (except when there is a dust storm or other aerosol episodes), low humidity, low precipitation, and small atmospheric and surface variability (Xiao *et al.* 2001, Yi *et al.* 2001, Hu *et al.* 2001a)

Since the two sensors have different overpass times, only clear scenes as observed by both sensors were employed. All images from the two sensors, beginning July 2002 until the end of October 2002, were searched and 11 pairs of cloud-free images were chosen. The dates and viewing geometries of the scenes are shown in table 4. Note that some of the pairs have large differences in viewing direction between the two sensors, especially on 15 July, 21 August, 26 August, 15 September and 13 October, when one sensor is viewed backward and the other viewed forward. This difference could incur larger calibration errors without an accurate BRDF correction. The most favourable cases were the last three days when the two sensors had the closest viewing directions.

From the selected pairs of images, we first cropped out the sub-images of the Dunhuang region in the Gobi desert. Seven to 15 ground control points (GCPs) were marked on both images using landmarks along the edge of the Gobi desert. The two images were then matched by a spatial transformation method using the GCPs. The original and matched images are shown in figure 2. The mean values

Table 4. Collocated imageries and their solar and viewing geometries.

| Date (Year 2002) | FY-1D | | | MODIS | | |
|---------------------|---------------------|--------------------|-------------------------|---------------------|--------------------|-------------------------|
| | Solar zenith (°) | View zenith (°) | Relative azimuth (°) | Solar zenith (°) | View zenith (°) | Relative azimuth (°) |
| 15 July | 35.2 | 33.2 | 174.5 | 27.2 | 42.9 | 83.1 |
| 21 August | 42.8 | 23.2 | 164 | 32.2 | 15.4 | 44.2 |
| 23 August | 46.1 | 2.2 | 19.5 | 34.2 | 35.0 | 43.7 |
| 26 August | 51.1 | 37.0 | 13.8 | 31.9 | 18.1 | 127.3 |
| 15 September | 50.1 | 11.1 | 156.6 | 40.4 | 25.9 | 52.9 |
| 1 October | 59.4 | 37.6 | 28.3 | 45.8 | 26.4 | 57.8 |
| 8 October | 55.3 | 23.1 | 147.5 | 47.8 | 16.3 | 59.6 |
| 13 October | 62.7 | 37.8 | 32.6 | 48.7 | 17.2 | 114.6 |
| 22 October | 61.6 | 2.9 | 50.9 | 52.0 | 6.3 | 114.5 |
| 24 October | 64.4 | 27.4 | 36.1 | 53.3 | 16.1 | 63.3 |
| 26 October | 67.5 | 46.4 | 35.3 | 54.8 | 35.8 | 71.3 |

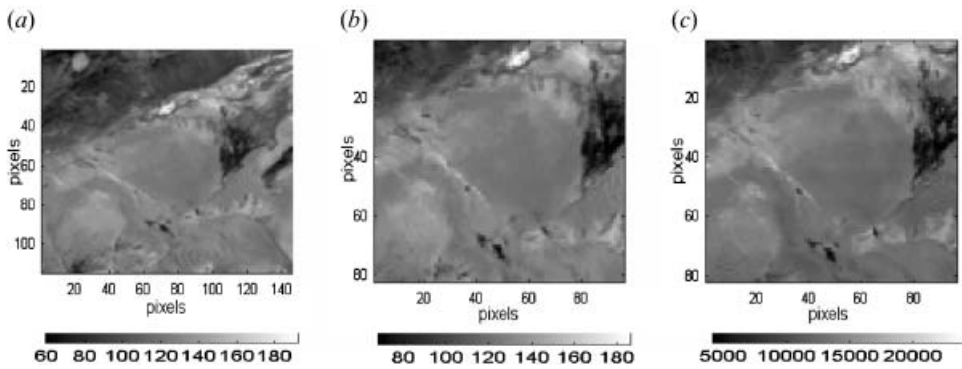


Figure 2. Registered images of FY-1D and MODIS on 8 October 2002 over the Dunhuang calibration site. (a) Original image of FY-1D channel 1, (b) FY-1D image registered to MODIS image, (c) image of MODIS band 1.

(radiance from MODIS and digital readings from MVIRS) over a small sub-area of 3×3 pixels in the most uniform portion of the desert were obtained from the matched sub-images and were used in subsequent analyses.

3. Calibration approach

In addition to the discrepancies in viewing geometry, the spectral bands of the MODIS and the MVIRS also differ. Broadly speaking, the first 10 MODIS channels (table 3) encompass the same spectral range as the MVIRS. However, the centres and bandwidths of the MODIS and MVIRS channels differ considerably. Cross-calibration must take into account the differences in both viewing geometry and spectral bands between the two sensors. The differences caused by the viewing geometry can be accounted for by the BRDF. The surface BRDF was measured in 1999 with an ASD spectrometer with a narrow FOV (1°). The spectrometer was mounted 6m above the ground on an auto-scanning device manufactured by the Anhui Optical and Fine Mechanical Institute.

Measurements were acquired with the viewing zenith angle scanning from 0° to 70.2° (increasing by 5.4° with each step) and the 23 relative azimuth angles covering the principle plane. A reflectance reference panel was measured at the 0° viewing zenith angle. The hemispherical scanning was completed in about 6 minutes. The BRDF data used here were measured over the calibration site on 7 July 1999, from 5:22 UTC to 9:21 UTC. Twenty-three datasets of hemispherical scanning measurements were obtained with the solar zenith angle ranging from 18° to 51° . Examples of the BRDF corresponding to MODIS bands 1 and 10 are shown in figure 3. It shows a general increasing trend towards the backward scattering direction; the other bands have similar trends. The small-scale scraggy surface likely results from the influence of the small-scale (< 20 cm) non-uniformity of the surface, which is sensitive to the narrow FOV of the instrument. To alleviate its impact on cross-calibration and extrapolating BRDF for a solar zenith angle larger than 51° , the BRDF measurements were fitted with the kernel-driven BRDF model proposed by Roujean *et al.* (1992). The model has been used successfully to account for the BRDF of AVHRR channels over various terrestrial surfaces (Wu *et al.* 1995, Li *et al.* 1996). The noise-like artefacts were smoothed out by fitting this model to the BRDF measurements (see, for example, figure 3(b,d)).

Application of the fitted surface BRDF to the satellite data requires an

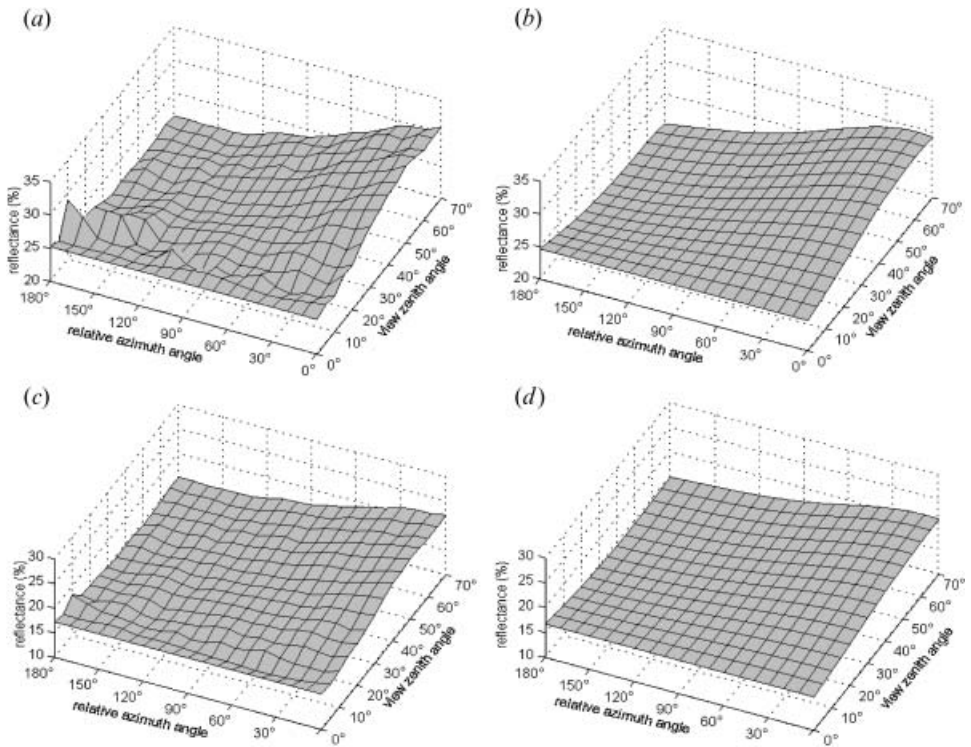


Figure 3. The BRDF of Dunhuang calibration site for MODIS band 1 (620–670 nm) and band 10 (483–493 nm) at a solar zenith angle of 39.6° . (a) Measured BRDF, MODIS band 1, (b) model fitted BRDF, MODIS band 1, (c) measured BRDF, MODIS band 10, (d) model fitted BRDF, MODIS band 10.

atmospheric correction, which is implemented using the 6S radiative transfer model. The model generates surface reflectances from TOA radiances by specifying atmospheric and surface conditions. In light of the atmospheric environment of the region and season, we adopted the standard mid-latitude summer model atmosphere with a desert aerosol model and visibility of 45 km. Substituting the MODIS radiances and the selected atmospheric model into the 6S model, the surface reflectances were estimated. The reflectances measured from the MODIS viewing angles (solar and satellite zenith angles and relative azimuth) were then converted into the solar-viewing geometry of the MVIRS. A comparison of the two sets of reflectances is presented in figure 4. Their differences denote the sole influence of the BRDF correction. The correction is quite significant and may be positive or negative depending on differences between the viewing geometries of the two sensors. The impact of the correction on the derivation of calibration coefficients is discussed later.

The BRDF-corrected surface reflectances were interpolated with a spline function to obtain a continuous surface reflectance spectrum. The smooth curve shown in figure 1 implies that no serious errors are likely introduced by the interpolation. Using the normalized band response functions of the MVIRS, the BRDF-modified and interpolated spectral reflectances were further converted to TOA values using the same 6S radiance transfer code and the same atmospheric conditions used before. The resulting TOA radiances now have the same viewing

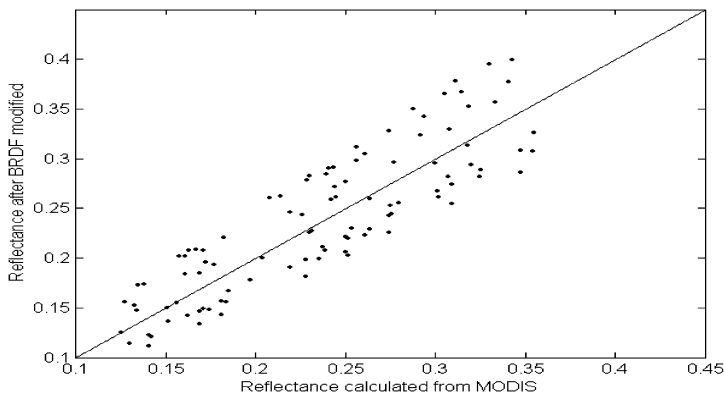


Figure 4. Surface reflectance estimated from MODIS before and after the BRDF correction.

geometry and spectral bands as the FY-1D MVIRS but the values are calibrated against the MODIS measurements. The entire processing scheme is summarized in figure 5.

Figure 6 presents the relationships between the predicted radiances and the satellite digital readings for all of the MVIRS solar channels. The two quantities are highly correlated in a linear manner, although the correlation splits into two groups for bands 1, 2 and 6, signifying an abrupt change in the calibration gain. According to the China National Satellite Meteorology Center, no calibration adjustment was made to the MVIRS during this period. The discontinuity appears to be real drift in the sensor's gain, as the data is separated into two observation periods. Similar abrupt change in calibration also happened to the METEOSAT in 1987 (Mamoudou *et al.* 2001). Were it not for an artefact, the data would be more likely mixed in date. The tight correlation corroborates the merits of the various correction procedures that we introduced. For example, the benefits of the BRDF correction are readily discernible by comparing correlations among the MODIS measurements (the + points in the figure) with those of the predicted MVIRS values at these bands (the * points in the figure). Note that the systematically higher MODIS values originate from the higher sun angles (see, for example, table 4), because the Terra overpass time is closer to the local noon time by about 1 to 2 hours than the FY-1D. The systematic differences have little to do with either the BRDF correction or the discrepancy in band response function. The scattering around the linear correlation line is indicative of the BRDF effect.

From the linear relationship between the predicted MVIRS radiances and their digital readings, one could simply derive the gains as the slopes of the linear regression lines. But this would prohibit us from gleaning information concerning any potential drift of the gains. We therefore elected to derive an individual gain from each measurement and then analyse its trend with respect to observational data. Using observations of dark space from the MVIRS as another point, the sensor's gains can be computed for all the matched data using the following equation:

$$R(i) = G(i)(DN - DN_0) \quad (1)$$

where $R(i)$ stands for predicted TOA radiance in the i th band of the MVIRS and G for the gain. DN and DN_0 are digital numbers corresponding to the two readings for the target and dark space, respectively.

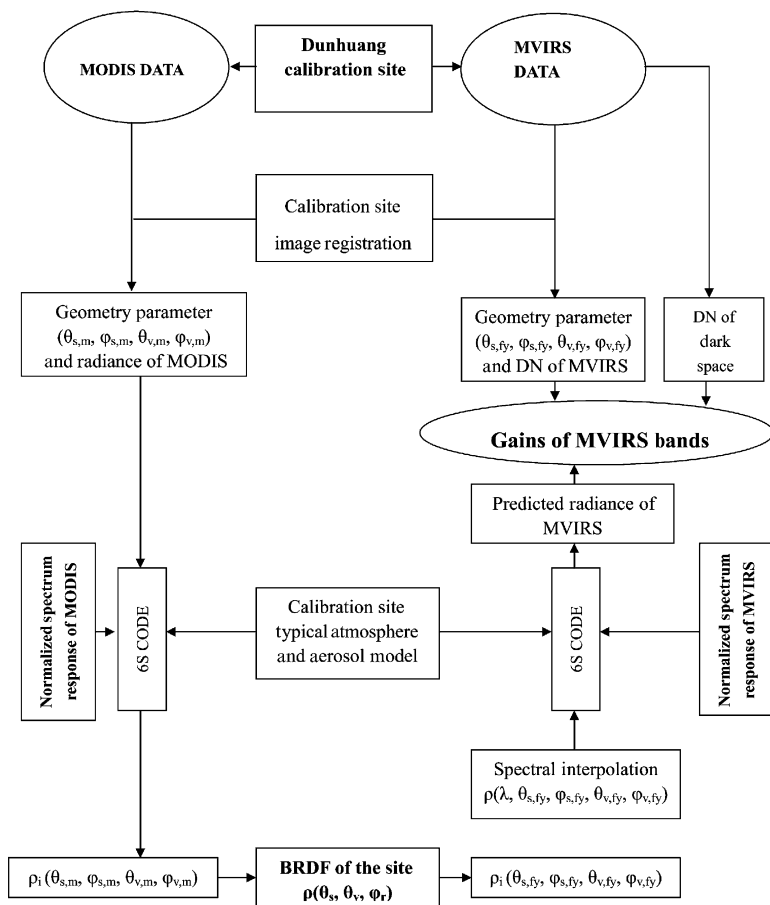


Figure 5. A flowchart of the cross calibration procedure.

The results are shown in figure 7. It is interesting to note that the gain values for channels 1 and 2 remain distinct between the two observation periods, but the values for channel 6 are united by a single regression line with data points tightly clustered around the line. For almost all the channels, the linear trends are so well-behaved that they bolster certain confidence to the calibration method and the gain values. The time-dependent gain functions are given by:

$$G(i) = K_1(i) + K_2(i)ND$$

where ND denotes the number of days since the sensor was launched. K_1 and K_2 are the linear regression coefficients whose values are given in table 5.

Recall that the FY-1D was launched on 15 May 2002. The new gains are compared with the pre-launch values that are marked on figure 7 as individual points corresponding to day ‘0’. Two months after launch it was found that the gains for some channels had drifted quite dramatically, while others were stable. There seems to be a complex relation between the pre-launch and post-launch values. For channels 1, 2 and 10, the pre-launch values are fairly compatible with the post-launch ones in the earlier periods of the calibration. However, for the remaining channels, they differ substantially. The gain values decrease for channel 6 and increase for channels 8 and 9 noticeably. The largest degradations occurred in

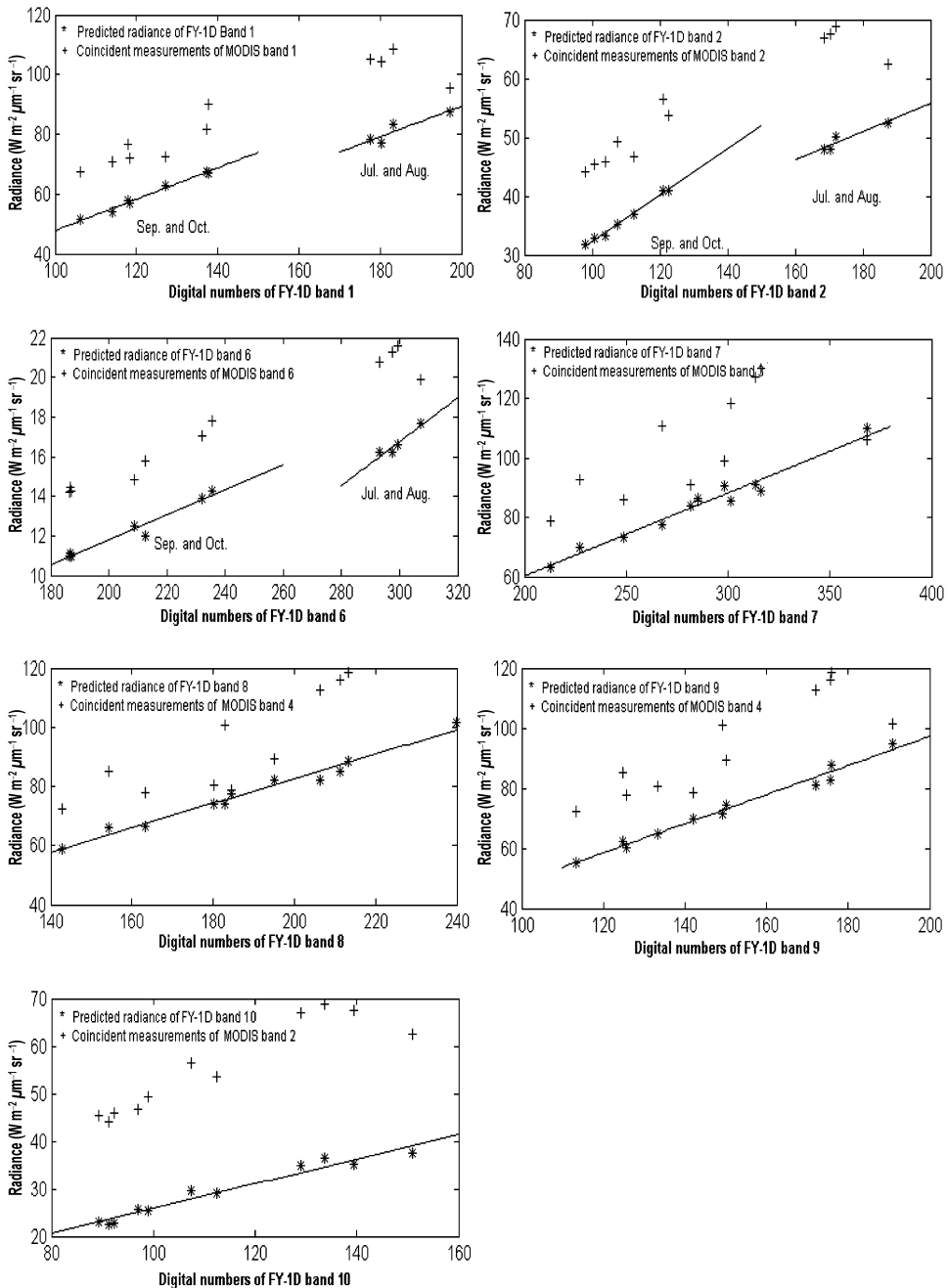


Figure 6. Relationships between the predicted radiances and satellite digital readings of FY-1C.

the latter two channels with relative changes of 34.7% and 47.3%, respectively. Drastic changes after launch are not surprising, which is a typical behaviour seen in similar sensors (e.g. NOAA-14). The magnitudes of the drifts observed here are not unusual. However, the rate of change over the three months of investigation is

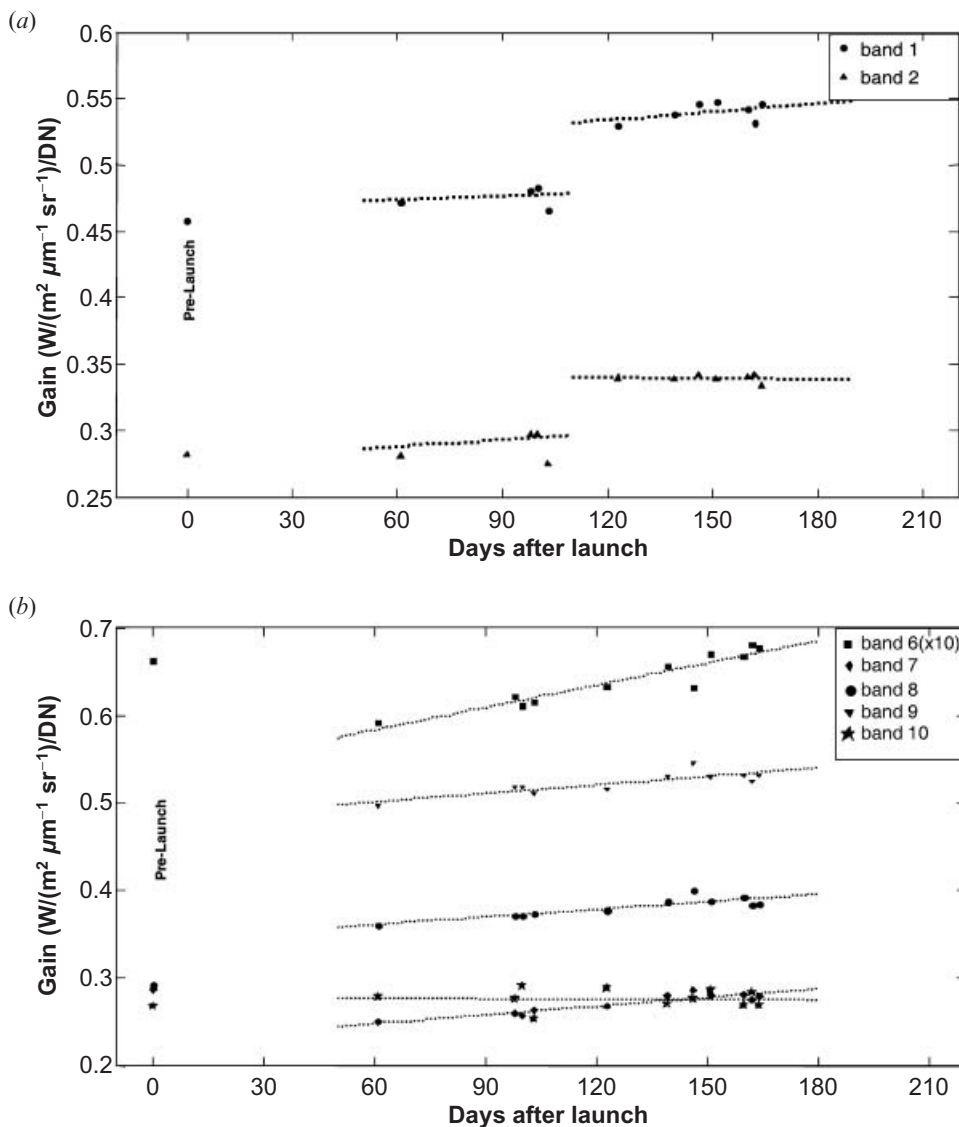


Figure 7. Temporal change in the gain of MVIRS for the first 5 months in orbit. (a) Gains of FY-1D bands 1, 2, (b) gains of FY-1D.

rather dramatic for some channels (e.g. channel 6). Long-term continual monitoring of the gain change is thus warranted.

4. Error analysis

As the flowchart in figure 5 shows, the cross-calibration procedure involves several steps, each of which may incur errors, reducing the accuracy of the calibration gain. It is not a trivial task to rigorously quantify them, but a 'best estimate' is attempted here to provide a rough idea of the magnitude of the potential errors. Individual sources of error are listed as follows:

Table 5. Linear regression coefficients for the gains change with time.

| Band | K_1 | K_2 | Standard deviation from the regression line (%) |
|-----------------------|-----------|------------|---|
| 1 (July–August) | 4.5689e-1 | 8.3504e-5 | 1.29 |
| 1 (September–October) | 4.8132e-1 | 2.0682e-4 | |
| 2 (July–August) | 2.4875e-1 | 1.7217e-4 | 2.18 |
| 2 (September–October) | 3.4617e-1 | -2.2348e-5 | |
| 6 | 4.1789e-2 | 8.4758e-5 | 1.59 |
| 7 | 1.8299e-1 | 3.3215e-4 | 1.68 |
| 8 | 3.0408e-1 | 2.9068e-4 | 1.47 |
| 9 | 4.3707e-1 | 3.2605e-4 | 1.34 |
| 10 | 2.7971e-1 | -1.3759e-5 | 3.90 |

1. *The uncertainty of the MODIS calibration:* The uncertainty of the MODIS calibration is about 2.2% to 3% (MODIS ATBD v2.0, 1997).
2. *Image co-registration error:* Any inaccurate registration between the images acquired by the two sensors introduces errors to the calibration. Given the exceptional uniformity of the surface in the central region of the Gobi desert, the maximum deviation of digital numbers from the two sensors is less than 1%. The calibration results are immune, to some extent, to mis-registration errors as long as they fall within the central 20-km area. Concerning *in situ* measurements of surface reflectance, the uncertainty due to image registration is estimated to be less than 1%.
3. *Atmospheric correction:* The assumed parameters for atmospheric correction in the radiative transfer code may add errors, but they are unlikely to be significant. As Teillet *et al.* (1990) demonstrated, calculations of two-way transmittance for downward and upward radiances using the same input parameters are subject to very small errors because of the error compensation in the two subsequent calculations. Based on their simulations and ours, the final error caused by atmospheric parameters is less than 1%.
4. *Spectral interpolation:* As shown in figure 1, this step is expected to have a minor effect. Nevertheless, we attempted to quantify it by comparing the observed radiances with the predicted radiances by means of radiative transfer calculations and spectral interpolation. The results show that the error is of the same order as that of the radiative transfer model, namely 1%.
5. *The BRDF correction:* This is one of the most critical steps in the cross-calibration process presented here and is thus likely a major source of uncertainty. Assuming that the errors in table 5 were mainly due to this and considering the range of the viewing zenith angle (near nadir to more than 40°) and the relative azimuth angle (covering both forward and backward scanning directions), we would expect the error to be less than 2% to 3%.

While the above estimates of individual errors may not be rigorous due to the lack of information to quantify them more precisely, the overall level of uncertainty is constrained by the tightness of the clusters shown in figures 6 and 7 and table 5. Note that the above errors are independent of each other, contributing to more random-like distributions in the matched data. The degree of randomness, as indicated by the scattering along the linear regression lines, is very small. From the relative standard deviation, we estimate that the total uncertainty of the calibration method ranges from 3.5% to 5%, which takes into account the uncertainty in

MODIS calibration as well. These uncertainties are better than those from the conventional calibration methods as used by Liu *et al.* (2002) and Hu *et al.* (2001). Moreover, the cost of the cross-calibration procedure is much lower so this procedure can be readily implemented for operational use.

5. Conclusion

China has launched and is operating both polar-orbiting and geostationary meteorological satellites. While freely receivable through AVHRR stations, data from these satellites have been severely under-utilized by the international community, due in part to a lack of knowledge concerning the calibration of the sensors. The MVIRS sensor aboard the Chinese sun-synchronous satellite (FY-1 series) has similar channels to the AVHRR but contains four extra channels and has a different overpass time from the AVHRR. As an alternative to the conventional vicarious calibration approach, this study presents a calibration method that can transfer the calibration of the MODIS to the MVIRS. To account for discrepancies in spectral coverage and viewing geometries between the two sensors, atmospheric radiative transfer modelling was used to derive surface bidirectional reflectance. The reflectance measured from the MODIS viewing geometry was converted to the viewing geometry of the MVIRS using a surface bidirectional reflectance distribution function (BRDF). Surface BRDF measurements were made in a calibration campaign over a uniform calibration site over a Gobi desert region in western China. The BRDF corrected reflectance values are further subject to spectral correction to account for differences in the spectral bands of the two sensors.

After various corrections, radiance values calibrated against the MODIS of the same viewing geometry and spectral coverage as the MVIRS are very tightly and linearly correlated with the MVIRS digital readings, allowing us to derive the calibration gains at the seven solar channels of the MVIRS. About two months after the launch of the MVIRS platform, the gains at some channels deviated considerably from the pre-launch values, with the largest degradation occurring at channels 8 and 9 (relative changes of 34.7% and 47.3%, respectively). These drastic changes appear to be related to the launch, as the gain changes over the study period of three months (July–October in 2002) are much less. The gain values for all channels except channels 1 and 2 show slightly linear decreases with time. The gains for channels 1 and 2 display two distinct sets of values over the first and second halves of the study period. An error analysis indicates that the calibration is accurate to within 5%, which is comparable to, or better than, the vicarious calibration method. The much lower cost of the new method makes it particularly tailored for routine long-term application, provided that the high standard of the MODIS calibration is maintained.

Acknowledgments

We thank Dr Wenjian Zhang (China Meteorological Administration), Dr N. Loeb (NASA/LaRC) and Mr Yi Weining (Anhui Institute of Optical and Fine Mechanics) for providing their help. The study is sponsored by a NASA grant NNG04GE79G, the China Scholarship Council and the National Science Foundation of China (40028503).

References

- BARBIERI, R., 1997, Draft of the MODIS Level 1B algorithm theoretical basis document version 2.0, ATBMOD-01.
- BARNES, W. L., PAGANO, T. S., and SALOMONSON, V. V., 1998, Prelaunch characteristics of the Moderate Resolution Imaging Spectroradiometer (MODIS) on EOS-AM1. *IEEE Transactions on Geoscience and Remote Sensing*, **36**, 1088–1100.
- BARNES, W. L., XIONG, X., and SALOMONSON, V., 2003, Status of Terra MODIS and Aqua MODIS. *Advances in Space Research*, **32**, 2099–2106.
- GUTMAN, G. G., 1999, On the use of long-term global data of land reflectances and vegetation indices derived from the Advanced Very High Resolution Radiometer. *Journal of Geophysical Research*, **106**, 6241–6256.
- HU, X., ZHANG, Y., QIU, K., ZHANG, L., and RONG, Z., 2001a, Optical and radiometric characteristics of CRCS. *Proceedings of China Remote Sensing Sensors Radiometric Calibration* (Beijing: Ocean Press), pp. 156–165.
- HU, X., ZHANG, Y., QIU, K., HUANG, Y., and ZHANG, G., 2001b, In-flight radiometric calibration for VIR channels of FY-1C satellite sensor by using irradiance-based method. *Proceedings of China Remote Sensing Sensors Radiometric Calibration* (Beijing: Ocean Press), pp. 249–257.
- KAUFMAN, Y., and HOLBEN, B. N., 1993, Calibration of the AVHRR visible and near-IR bands by atmospheric scattering, ocean glint and desert reflection. *International Journal of Remote Sensing*, **14**, 21–52.
- LI, Z., CIHLAR, J., ZHANG, X., MOREAU, L., and HUNG, L., 1996, The bi-directional effect in AVHRR measurements over boreal regions. *IEEE Transactions on Geoscience and Remote Sensing*, **34**, 1308–1322.
- LIU, J., XIAO, Q., YU, H., and ZHANG, H., 2001, Airborne radiance based radiometric calibration test for the in-orbit remote sensing sensors. *Proceedings of China Remote Sensing Sensors Radiometric Calibration* (Beijing: Ocean Press), pp. 237–248.
- LYU, C., and BARNES, W., 2003, Four years of TRMM/VIRS on-orbit calibration and performance using lunar models and data from Terra/MODIS. *Journal of Atmospheric and Oceanic Technology*, **20**, 333–347.
- MAMOUDOU, B., FROUIN, R., NICHOLSON, E., and DEDIEU, G., 2001, Satellite-derived surface radiation budget over the African continent. Part I: Estimation of downward solar irradiance and albedo. *Journal of Climate*, **14**, 45–58.
- RAO, C. R. N., and CHEN, J., 1995, Inter-satellite calibration linkages for the visible and near-infrared channels of the Advanced Very High Resolution Radiometer on the NOAA-7, -9, and -11 spacecraft. *International Journal of Remote Sensing*, **16**, 1931–1942.
- ROUJEAN, J. L., LEROY, M., and DESCHAMPS, P. Y., 1992, A bi-directional reflectance model of the Earth's surface for the correction of remote sensing data. *Journal of Geophysical Research*, **97**, 20455–20468.
- SLATER, P. N., and BIGGAR, S. F., 1996, Suggestions for radiometric calibration coefficient generation. *Journal of Atmospheric and Oceanic Technology* Special issue on EOS calibration, **13**, 376–382.
- SLATER, P. N., BIGGAR, S. F., THOME, K. J., GELLMAN, D. I., and SPYAK, P. R., 1996, Vicarious radiometric calibrations of EOS sensors. *Journal of Atmospheric and Oceanic Technology*, **13**, 349–359.
- TEILLET, P. M., SLATER, P. N., DING, Y., SANTER, R. P., JACKSON, R.D., and MORAN, M. S., 1990, Three methods for the absolute calibration of the NOAA AVHRR sensors in-flight. *Remote Sensing of Environment*, **31**, 105–120.
- VERMOTE, E., and KAUFMAN, Y. J., 1995, Absolute calibration of AVHRR visible and near-infrared channels using ocean and cloud views. *International Journal of Remote Sensing*, **16**, 2317–2340.
- VERMOTE, E., TANRÉ, D., DEUZÉ, J. L., HERMAN, M., and MORCETTE, J. J., 1997, Second simulation of the satellite signal in the solar spectrum: an overview. *IEEE Transactions on Geoscience and Remote Sensing*, **35**, 675–686.
- WU, A., LI, Z., and CIHLAR, J., 1995, Effects of land cover type and greenness on AVHRR bidirectional reflectance: analysis and removal. *Journal of Geophysical Research*, **100**, 9179–9192.
- XIAO, Q., LIU, J., YU, H., and ZHANG, H., 2001, Analysis and evaluation of optical uniformity for Dunhuang calibration site by airborne spectrum survey date.

- Proceedings of China Remote Sensing Sensors Radiometric Calibration* (Beijing: Ocean Press), pp.136–142.
- XIONG, X., CHIANG, K., ESPOSITO, J., GUENTHER, B., and BARNES, W., 2002, MODIS on-orbit calibration and characterization. *Metrologia*, **40**, 89–92.
- YI, W., QIAO, Y., WANG, X., ZHANG, J., ZHANG, Y., and WANG, L., 2001, Reflectance and atmospheric optical character of Dunhuang and Lake Qinghai radiometric calibration test site. *Proceedings of China Remote Sensing Sensors Radiometric Calibration* (Beijing: Ocean Press), pp.167–176.
- ZHANG, Y., ZHANG, G., HUANG, Y., QIU, K., HU, Y., WANG, W., LIU, Z., PONG, Z., ZHANG, L., ZHU, X., WANG, Y., LI, C., XIA, Q., CHEN, X., and FANG, Z., 2001, In flight vicarious radiometric calibration for VIS-SWIR channels of FY-1C satellite sensor at Dunhuang site. *Proceedings of China Remote Sensing Sensors Radiometric Calibration* (Beijing: Ocean Press), pp.266–274.